

4D Electrical Resistivity Imaging of Stress Perturbations Induced During High-Pressure Shear Stimulation Tests

Tim C Johnson¹, Jeffrey Burghardt¹, Christopher Strickland¹, Dana Sirota², Vince Vermeul¹, Hunter A Knox³, Paul C Schwering⁴, Doug Blankenship⁴, and Timothy J Kneafsey⁵

¹Pacific Northwest National Laboratory (DOE)

²Pacific Northwest National Laboratory

³Pacific Northwest National Lab

⁴Sandia National Laboratories

⁵Lawrence Berkeley Laboratory

January 24, 2024

Abstract

Fluid flow through fractured media is typically governed by the distribution of fracture apertures, which are in turn governed by stress. Consequently, understanding subsurface stress is critical for understanding and predicting subsurface fluid flow. Although laboratory-scale studies have established a sensitive relationship between effective stress and bulk electrical conductivity in crystalline rock, that relationship has not been extensively leveraged to monitor stress evolution at the field scale using electrical or electromagnetic geophysical monitoring approaches. In this paper we demonstrate the use time-lapse 3-dimensional (4D) electrical resistivity tomography to image perturbations in the stress field generated by pressurized borehole packers deployed during shear-stimulation attempts in a 1.25 km deep metamorphic crystalline rock formation.

Hosted file

985263_0_art_file_11801033_s7kxkq.docx available at <https://authorea.com/users/534176/articles/705540-4d-electrical-resistivity-imaging-of-stress-perturbations-induced-during-high-pressure-shear-stimulation-tests>

1

2 **4D Electrical Resistivity Imaging of Stress Perturbations Induced During High-** 3 **Pressure Shear Stimulation Tests**

4 **T. C. Johnson¹, J. Burghardt¹, C. Strickland¹, D. Sirota¹, V. Vermeul¹, H. Knox¹, P.**
5 **Schwering², D. Blankenship² and T. Kneafsey³ and the EGS Collab Team**

6 ¹Pacific Northwest National Laboratory, Richland Washington, USA

7 ²Sandia National Laboratories, Albuquerque New Mexico, USA

8 ³Lawrence Berkeley National Laboratory, Berkeley California, USA

9

10 Corresponding author: Tim Johnson (tj@pnnl.gov)

11 **Key Points:**

- 12 • Remotely monitoring stress is challenging but important for relating geomechanical
13 behavior to flow pathways during energy production
- 14 • Bulk electrical conductivity is sensitive to stress in crystalline rock
- 15 • Time-lapse electrical resistivity tomography can be used to remotely monitor 3D changes
16 in effective stress

17

18 **Abstract**

19 Fluid flow through fractured media is typically governed by the distribution of fracture apertures,
20 which are in turn governed by stress. Consequently, understanding subsurface stress is critical
21 for understanding and predicting subsurface fluid flow. Although laboratory-scale studies have
22 established a sensitive relationship between effective stress and bulk electrical conductivity in
23 crystalline rock, that relationship has not been extensively leveraged to monitor stress evolution
24 at the field scale using electrical or electromagnetic geophysical monitoring approaches. In this
25 paper we demonstrate the use time-lapse 3-dimensional (4D) electrical resistivity tomography to
26 image perturbations in the stress field generated by pressurized borehole packers deployed
27 during shear-stimulation attempts in a 1.25 km deep metamorphic crystalline rock formation.

28

29 **Plain Language Summary**

30 Time-lapse electrical geophysical sensing is used to image 3D changes in rock stress generated
31 by an isolated and pressurized interval of a borehole in a deep, dense, fractured rock formation.

32

33 **1 Introduction**

34 Enhanced Geothermal Systems (EGS) offer a tremendous potential source of clean baseload
35 energy to support the energy security of the United States (Augustine, 2016). EGS involves the

36 challenging task of establishing hydraulic connections between two or more boreholes in deep,
37 hot, dry rock, whereby fluid may be circulated to extract thermal energy. Successful EGS
38 development requires improved understanding and control of EGS reservoir stimulation, where
39 fractures are generated and/or enhanced to provide effective heat-exchanging flow pathways
40 between injection and production wells. Stimulation processes and long-term efficacy are
41 governed in large part by both the natural state of stress and the evolution of stress during
42 stimulation and operation (Min, Rutqvist, Tsang, & Jing, 2004; Zoback & Byerlee, 1975a,
43 1975b). Consequently, developing improved methods of understanding and monitoring stress are
44 important for EGS development (Pyrak-Nolte, 2015).

45 The EGS-Collab project was funded by the U.S. Department of Energy, Geothermal
46 Technologies Office, to conduct fracture stimulation studies in a highly instrumented field
47 research testbed at EGS-relevant stress states (T. Kneafsey, 2022). Experiment #1, which
48 focused on executing and monitoring hydrofracture stimulations, was conducted on the 4850
49 Level of the Sanford Underground Research Facility (SURF) in Lead, South Dakota,
50 approximately 1.5 km below ground surface (bgs) (Fu et al., 2021; Heise, 2015). In Experiment
51 #2, shear stimulation testing was conducted on the 4100 Level of SURF, which lies
52 approximately 1.25 km bgs (T. Kneafsey, 2022). Shear stimulation involves isolating and
53 pressurizing an existing fracture below the minimum principle stress (to avoid hydrofracturing)
54 in an attempt shear-slip the fracture and create a self-propped hydraulic connection between two
55 boreholes. Shear stimulation was attempted at approximately 10 candidate locations, none of
56 which resulted in a successful shear slip, or any fluid injected into the formation. In addition to
57 extensive pressure, flowrate, and fluid conductivity monitoring, each attempt was closely
58 monitored using 4D cross-borehole seismic, fiber-based distributed temperature and strain, and
59 4D electrical resistivity tomography (ERT).

60 In this paper, we demonstrate how 4D ERT monitoring was used to image stress-induced
61 perturbations in bulk electrical conductivity (BEC) during Experiment #2 shear stimulation
62 attempts at six different depths. During each stimulation attempt, a section of the borehole was
63 isolated and pressurized using a pair of straddle packers. Compressive stresses exerted on the
64 borehole wall by the packers and pressurized interval induced an effective stress perturbation
65 ‘bulb’ around the interval, and a consequent decrease in porosity (and therefore BEC) within the
66 stress bulb. The resulting decrease in BEC within the stress bulb was then imaged in 3D using
67 ERT electrodes deployed within surrounding monitoring boreholes. Although the sensitivity of
68 BEC to stress in crystalline rock is well documented at the laboratory scale (Brace, 1975; Brace
69 & Orange, 1966; Brace, Orange, & Madden, 1965; Kaselow & Shapiro, 2004), field-scale efforts
70 to infer stress evolution using electrical or electromagnetic geophysical methods are limited.
71 Because there was no flow within the formation during the stimulation attempts, changes in BEC
72 during stimulation are uniquely attributable to changes in stress. Comparisons of ERT images
73 collected between shear stimulation attempts and a follow-on hydrofracture simulation show that
74 the 3D stress perturbation patterns generated during shear stimulation attempts provided insight
75 regarding the hydrofracture location and orientation. In addition to demonstrating the field-scale
76 sensitivity of BEC to stress at EGS-relevant depths and pressures, results also point to the
77 possibility of new approaches for EGS monitoring and for inferring in-situ rock properties.

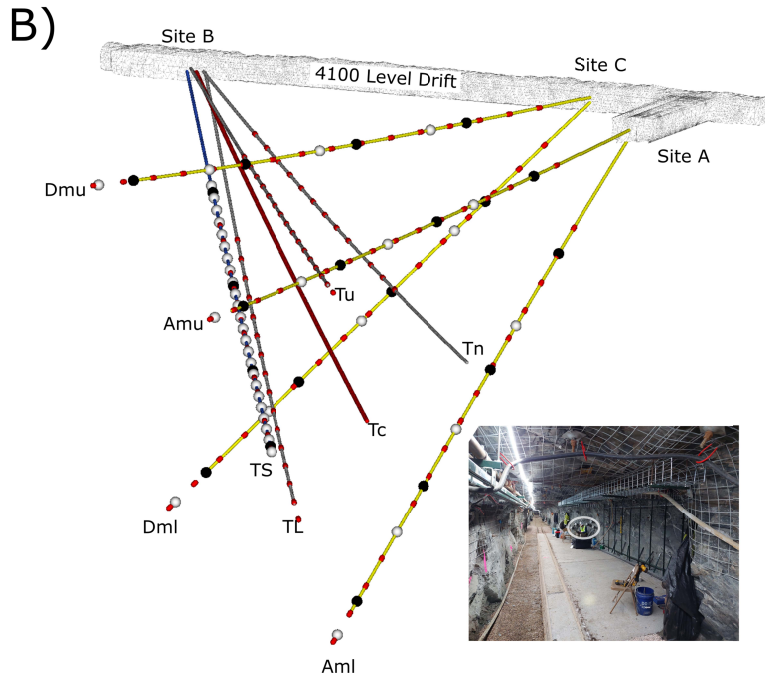
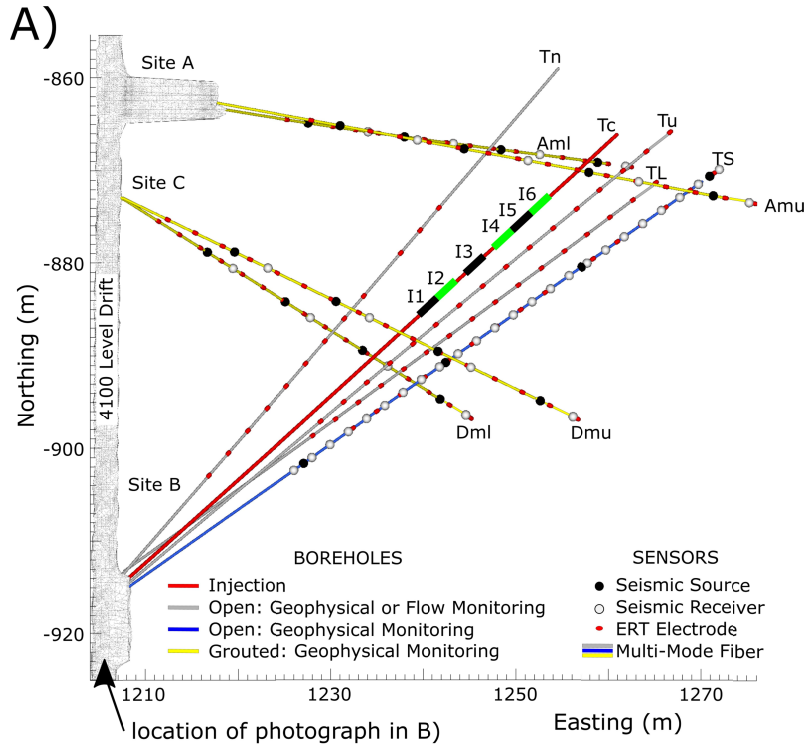
78 We begin by describing the Experiment #2 testbed and the shear stimulation sequences, which
79 end with a hydrofracture stimulation. We then present the ERT imaging results and
80 corresponding interpretation. Finally we conclude with a discussion of the results and possible

81 new avenues for inferring in-situ bulk modulus and intrinsic permeability using ERT monitoring
82 of stress perturbations.

83 2 EGS-Collab Experiment #2 Testbed

84 Experiment #2 of the EGS-Collab project was conducted on the 4100 Level of SURF, which lies
85 ~1.25 km (4100 ft) below the ground surface. Testing boreholes were installed within an
86 amphibolite sequence known as the Yates member of the Poorman Formation, consisting of
87 metamorphosed basalt to form a massive hornblende-plagioclase amphibolite schist, with lesser
88 amounts of quartz and calcite (Caddey, 1991). Figure 1 shows the testbed layout, consisting of
89 nine subhorizontal boreholes originating at the eastern wall of the drift. Four dedicated
90 geophysical monitoring boreholes originating at sites A and C (AMU, AML, DMU and DML)
91 were instrumented with seismic sources and receivers, multi-mode (temperature and strain)
92 sensing fiber, and ERT electrodes, all grouted in place. The remaining five boreholes originating
93 from site A were left open to enable multiple-use configurations including geophysical
94 instrumentation or zonal isolation packers for precisely-located pressure monitoring and flow
95 control. For Experiment 2, boreholes Tn, Tu, Ts and Tl were instrumented with ERT electrodes,
96 with Ts also including seismic sources and receivers. Borehole Tc was oriented to maximize the
97 probability of shear slip during stimulation, given what was known about the in-situ stress field
98 (Burghardt et al., 2022).

99 Shear stimulation attempts were conducted by isolating (using a straddle packer system) and
100 pressurizing targeted sections of Tc where potential shearable fracture intervals were identified
101 through core inspection. Here, we focus on shear stimulation intervals I1-I6 shown in Figure 1A.
102 Each interval (green or black) shows the corresponding pressurized interval for each test, which
103 includes the ~2 m pressurized interval bounded on each end by borehole packers. The inset
104 photograph in Figure 1B was taken inside the 4100 Level drift during testbed construction just
105 south of Site B facing northward to Site A.



106

107

108

109

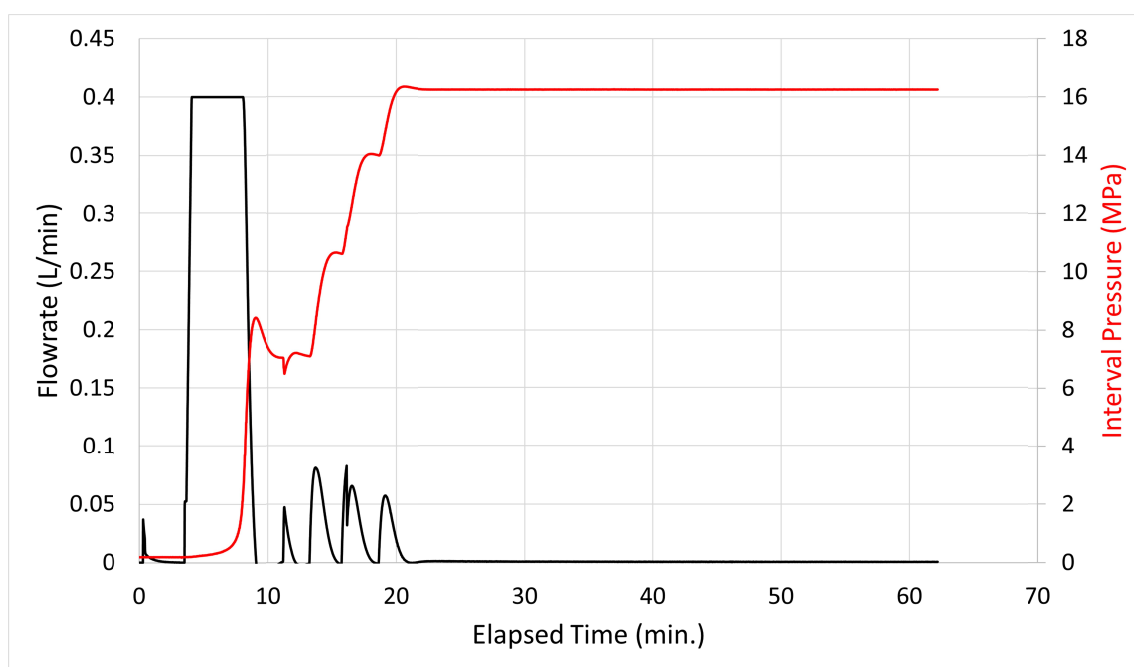
110

111

Figure 1. A) Plan and B) Oblique views of the experimental testbed including borehole orientations with ERT and seismic instrumentation locations. Intervals I1-I6 (black and green) in A) denote isolated sections of borehole Tc that were pressurized during shear stimulation attempts. The inset image in B) is a photograph taken during testbed construction, standing in the drift at -917 m northing and facing northward (as annotated in A). Kickoff points for Site B boreholes are located within the white outline.

112 3 Shear Stimulation Experiments

113 A primary objective of Experiment #2 was to shear-slip a natural fracture in borehole Tc and
 114 generate a self-propped hydraulic connection between Tc and one or more of the Site B
 115 boreholes. Each shear experiment proceeded by isolating a ~2 m interval of the borehole (Figure
 116 1, I1-I6) using a pair of straddle packers, each packer being ~1.5 m long for a total length of 5 m.
 117 After the pressure of each packer was raised to 10.34 MPa (1500 psi), the interval flowrate was
 118 recorded as the interval pressure was raised to 16.25 MPa (2350 psi), which is approximately
 119 83% of the previously estimated minimum principle stress (T. Kneafsey, 2022) and
 120 approximately 30% of the estimated interval pressure required to generate tensile stress at the
 121 interval wall. Interval pressure was then held at 16.25 MPa for at least 30 minutes while interval
 122 flowrate was recorded. In every case, zero interval flow was recorded during the hold period,
 123 indicating an unsuccessful shear stimulation attempt. Figure 2 shows a typical flowrate and
 124 interval pressure timeseries during a shear stimulation attempt, Tc interval I1 (Figure 1A) in this
 125 case.



126
 127 *Figure 2. Flowrate and interval pressure for shear stimulation attempt in wellbore Tc interval I1 (Figure 1A). Flowrate*
 128 *variations during the first ~20 minutes occur during interval pressure-up (i.e. there is no flow into the formation).*

129 4 ERT Monitoring During Stimulation Attempts

130 ERT data were collected in a pole-pole like configuration. A single measurement was collected
 131 by injecting current between one of the electrodes shown in Figure 1 and a remote electrode.
 132 During the current injection, the induced potential was measured between one or more of the
 133 electrodes shown in Figure 1 and a second remote electrode, which provided the potential
 134 reference for all measurements. As shown by the inset photograph in Figure 1B, continuous
 135 metallic wire mesh was installed on the ceiling and walls of the drift for rockfall protection,
 136 pinned to the rock using metallic rock bolts on a ~2m grid. Electrical coupling between the mesh,
 137 rock bolts, and rock effectively formed a zero-potential reference surface on the ceiling and walls

138 of the drift. With this in mind, we used the mesh as both the current sink and potential reference
139 electrode for all measurements.

140 Measurements were collected using an 8-channel ERT data acquisition system, meaning eight
141 potential measurements were collected for each current injection. Pre-stimulation baseline
142 surveys were collected continuously for two days and analyzed to remove data with small signal
143 to noise ratios, which were generally associated with measurements where the potential electrode
144 was far from the current electrode. For the 124 electrodes in the array, the full pole-pole survey
145 consisted of 7749 measurements. After filtering, 3615 of those measurements were deemed
146 outside of the noise envelope and were collected during the time-lapse imaging phase. The time
147 interval between ERT survey times, or equivalently between ERT images, was approximately 46
148 minutes.

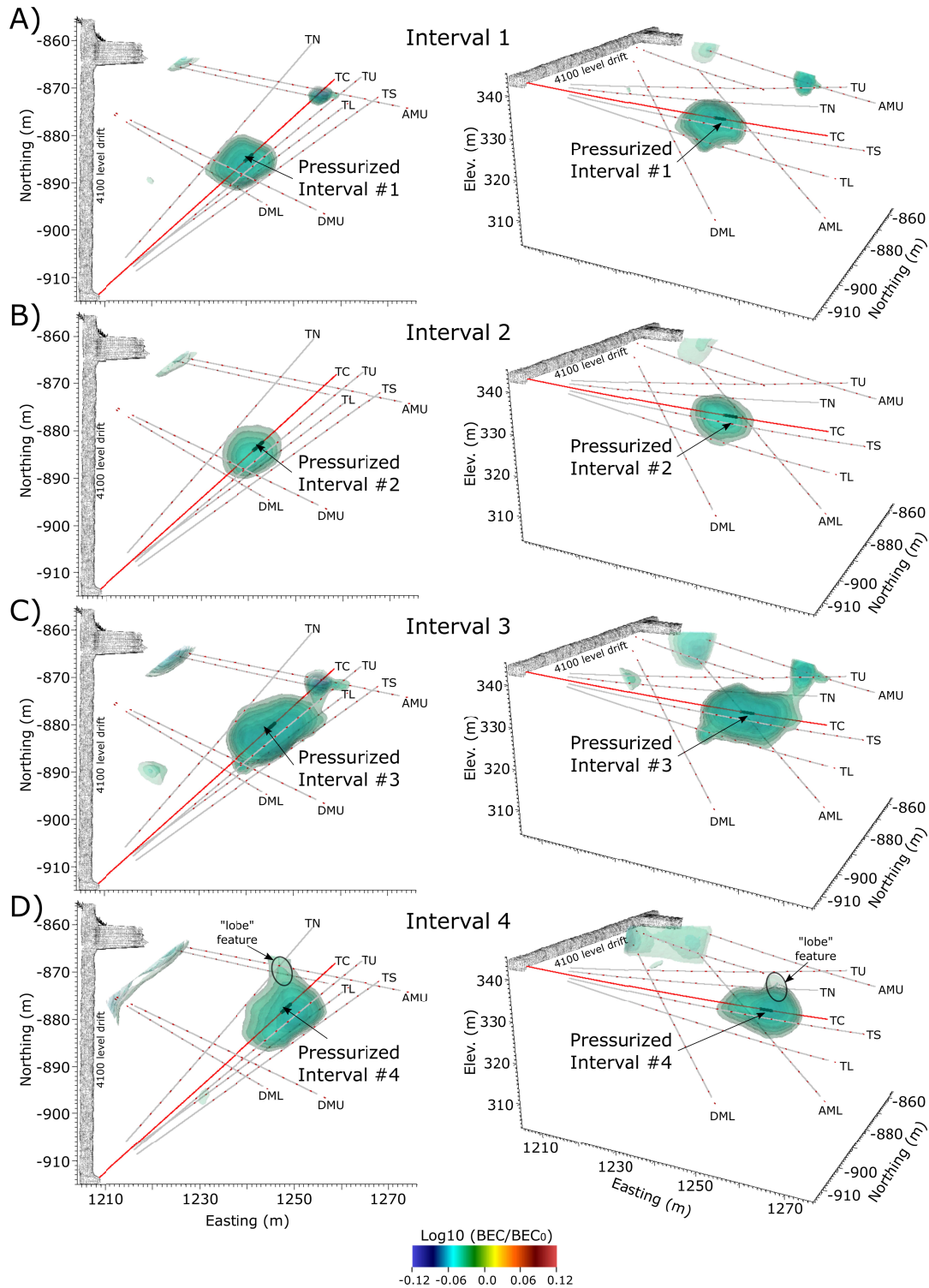
149 **5 ERT Data Processing**

150 Surveys were collected continuously during the shear stimulation attempts. After each survey,
151 data were autonomously transferred to offsite computing resources and processed. Data were
152 inverted in parallel on 66 processing cores using the open source E4D software
153 (<https://e4d.pnnl.gov>). The total time between the beginning of a survey and delivery of the
154 resulting ERT image was approximately 55 minutes. Drift boundaries were located using LiDAR
155 sensing, which enabled the drift boundaries to be precisely simulated using an unstructured
156 tetrahedral mesh. Elements inside of the drift boundaries were removed to simulate zero current
157 flux conditions across drift boundaries. Constant potential conditions along the drift walls and
158 ceilings caused by the rockfall protection mesh were simulated using the metallic infrastructure
159 modelling method described by (Johnson & Wellman, 2015).

160 Baseline BEC structure was established by inverting one of the ERT data sets collected prior to
161 the stimulation attempts. Occam's-type regularization constraints were imposed by enforcing
162 nearest-neighbor smoothing, whereby the difference in BEC between neighboring elements was
163 minimized, subject to fitting the data. Two different constraints were imposed to regularize the
164 time lapse inversions of data collected during shear stimulation events. First, the change in BEC
165 from the previous time-step between neighboring cells was minimized, which enforces
166 smoothness in the change in BEC in both space and time. Second, changes in BEC were
167 constrained to be negative with respect to baseline BEC conditions. The second constraint is
168 justified based on the assumption that unless fluid was injected into the formation, there was no
169 active mechanism to increase BEC during the time-lapse imaging. That is, we assumed no
170 increase in porosity, fluid conductivity, or temperature within the formation during the shear
171 stimulation attempts. To the contrary, the increased compressive stress with respect to baseline
172 imposed by the pressurized stimulation interval decreased porosity, leading to a corresponding
173 decrease in BEC (Brace & Orange, 1966; Brace et al., 1965). Had fluid been introduced into the
174 formation during the shear stimulation attempts, the inversion would have been re-run without
175 the negativity constraint, as was done with the time-lapse inversion of the hydrofracture
176 stimulation.

177 **6 ERT Imaging Results**

178 ERT imaging results for each of the six stimulation intervals are shown in Figures 3 and 4.
179 Changes in BEC from baseline are shown as iso-surfaces in plan and oblique views for each
180 stimulation event. In each case, changes in BEC are negative with respect to baseline conditions
181 and focus around the pressurized injection interval. Decreases in BEC mirror the anticipated
182 effective stress perturbation, in that the largest magnitudes occur at, and decay with distance
183 from, the pressurized interval. The relationship between stress and BEC can be described as
184 follows (Brace, 1975; Johnson et al., 2021; Kaselow & Shapiro, 2004):



185

186 *Figure 3. ERT-derived changes in BEC during shear stimulation attempts in intervals 1-4. Decreases in BEC are caused by*
 187 *stress-induced decreases in porosity around the pressurized interval.*

188 When the interval is pressurized, the surrounding host rock experiences a corresponding increase
 189 in total stress. In response, compliant microfractures compress, resulting in a decrease in
 190 porosity, and a corresponding decrease in BEC. The stress-induced decrease in porosity requires

191 that either the pore water compresses within the pore space, or the pore water migrates out of the
 192 pore space. Although measurements of host rock compressibility (or its inverse, bulk modulus)
 193 aren't available, we assume that, like other dense crystalline rocks, rock compressibility is less
 194 than that of water at the same temperature and pressure. For example, the compressibility of
 195 water at standard temperature and pressure is approximately $5E-10 \text{ GPa}^{-1}$ (Schmitt, 2015). In
 196 contrast, Davarpanah et al. (2020) reported the compressibility of unaltered granite and
 197 hornblende schist at approximately $2.9E-10 \text{ GPa}^{-1}$ and $1.3E-10 \text{ GPa}^{-1}$ respectively. If these
 198 compressibilities approximate testbed conditions, then it is reasonable to assume that the
 199 decrease in porosity occurred coincident with pore water compression, as opposed to pore water
 200 migration. The same assumption is supported by the lack of flow from the pressurized interval
 201 (Figure 2).

202
 203 Figure 4C shows the change in BEC from a survey collected during the hydrofracture stimulation
 204 and flow test in interval 4, after initiation of the hydrofracture. The fracture breakthrough point
 205 on wellbore AMU was recorded as a strain perturbation on distributed strain sensing (DSS) fiber
 206 at the location shown (Kneafsey et al., 2023). Like the shear stimulation attempt in interval 4
 207 (Figure 3D), a negative BEC anomaly develops around the pressurized interval. However, in this
 208 case, the anomaly is more elongated along the projection of the hydrofracture from interval 4 to
 209 AMU, and is presumably caused by the compressive stress exerted normal to the pressurized
 210 hydrofracture. Although the hydrofracture itself represents an increase in BEC from baseline, the
 211 ERT response is negative, and therefore dominated by the stress exerted on the host rock
 212 by the pressurized hydrofracture in this case.

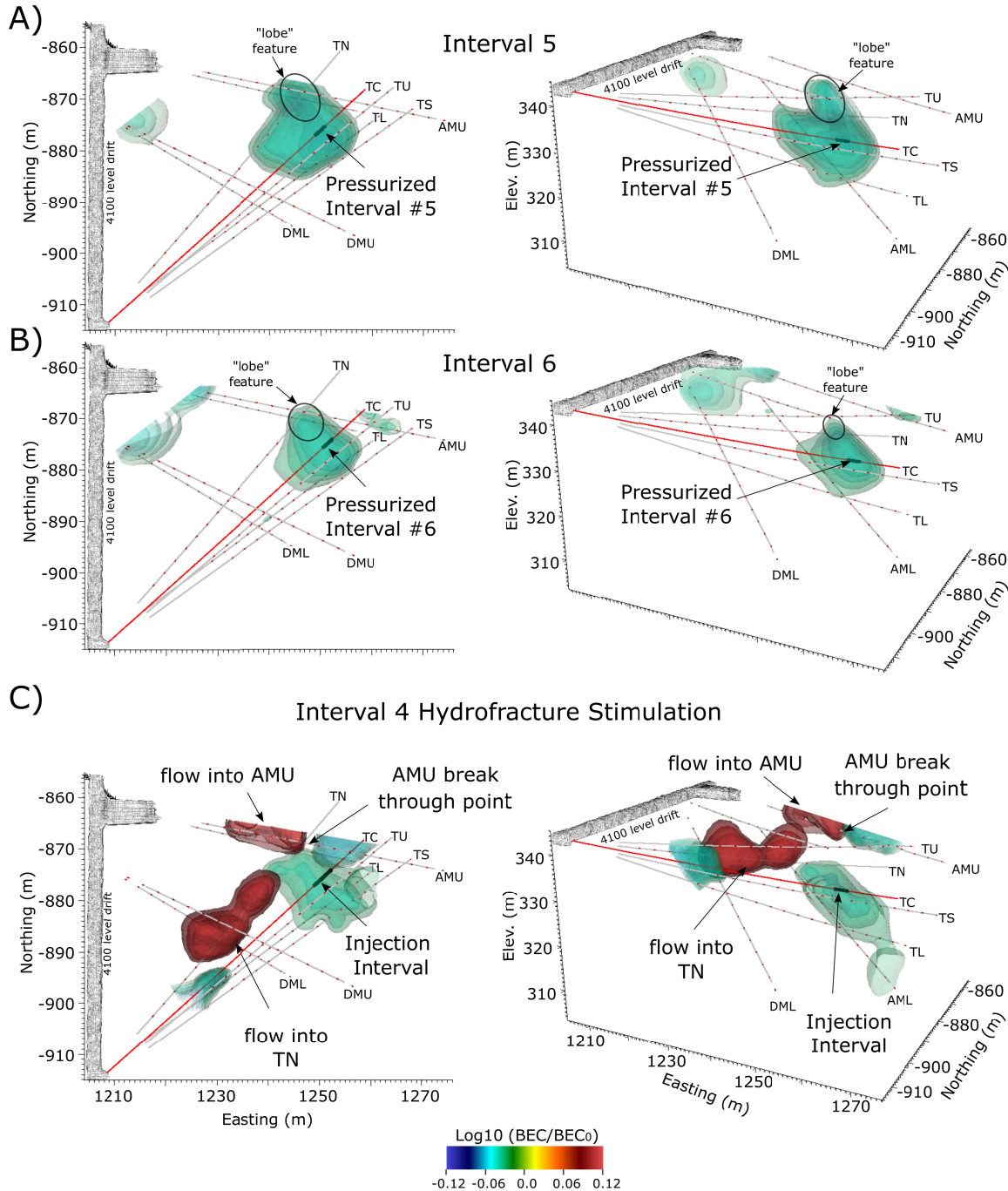
213
 214 Figure 4C also shows a BEC anomaly centered around borehole AMU that transitions from a
 215 positive BEC anomaly to a negative BEC at the point of the hydrofracture intersection. The
 216 shallower positive anomaly is caused by high-pressure fluid migrating from the hydrofracture
 217 into AMU and toward the drift. Although AMU was grouted, flow (dripping $\sim 10 \text{ ml/min}$) from
 218 AMU was observed shortly after stimulation, confirming that pressurized water was entering the
 219 borehole. The deeper negative anomaly surrounding AMU is presumably caused by
 220 compressive forces exerted normal to the pressurized hydrofracture on AMU, which is likely
 221 more compliant than the host rock. The consequent compression of AMU near the hydrofracture
 222 results in a decrease in porosity, and a subsequent decrease in BEC at the borehole.

223
 224 The positive BEC anomaly that develops around borehole TN is also caused by fluid inflow,
 225 confirmed by outflow from the wellhead in the drift. In contrast to borehole AMU, borehole TN
 226 was not grouted and open to atmospheric pressure. Inflow into TN suggests the hydrofracture
 227 intersected TN. However, unlike AMU, the point at which the hydrofracture intersects TN is not
 228 indicated by the BEC anomaly. The deepest point of the BEC anomaly surrounding TN occurs at
 229 the last electrode in TN (Figure 1A), which is the deepest point of sensitivity to fluid influx. The
 230 hydrofracture intersection with TN likely occurs deeper in the borehole.

231 232 **7 Discussion**

233
 234 The footprint of the BEC anomaly appears to vary considerably between shear stimulation
 235 attempts (Figure 3A-3D, Figure 4A-4B). Although this may be an artifact of variable spatial
 236 resolution caused by the non-uniform distribution of electrodes, it is the opinion of authors that

237 differences in the size of the BEC anomalies are caused by temporal ‘smearing’. In intervals 1, 2
 238 and 6, the time taken for a stimulation attempt was slightly less than the time required to
 239 complete a full ERT survey. Consequently, some fraction of ERT data were collected when the
 240 interval was not pressurized, which would naturally result in a smaller BEC anomaly.
 241



242
 243
 244 *Figure 4. ERT-derived changes in BEC during shear stimulation attempts in intervals 5 and 6 (4A and 4B) and during the*
 245 *hydrofracture stimulation (4C). Decreases in BEC are caused by stress-induced decreases in porosity around the pressurized*
 246 *interval. The annotated ‘lobe’ feature observed during shear stimulation attempts 4-6 (Figures 3D, 4A and 4B) is co-located with*
 247 *the projection of the hydrofracture from the injection interval to the break through point on wellbore AMU.*

248 The relative shape of the BEC anomaly also varies considerably between shear stimulation
249 attempts. Intervals 1 and 2 display a relatively uniform ovoid shape around the pressurized zone
250 with the long axis parallel to the borehole. In contrast, intervals 3-6 develop a lobe that extends
251 northward and vertically toward the TN and AMU boreholes. Notably, the lobe extending from
252 interval 4 follows the same trajectory as the hydraulic fracture stimulated from interval 4
253 (Figures 3D and 4C). This suggests that the BEC lobe was located in a zone of relatively
254 compliant rock that ultimately fractured during the interval 4 hydrostimulation. Upward and
255 northward trending BEC lobes extending from intervals 5 and 6 (Figure 4, upper two panels)
256 appear to be caused by the same region of comparatively decreased bulk modulus.

257 In addition to providing information regarding stress perturbations during the stimulation
258 attempts, time-lapse ERT may lead to new approaches for the in-situ measurement of intrinsic
259 permeability under low permeability conditions like those found in the Experiment #2 testbed.
260 For instance, consider the case where a borehole is instantaneously 'dry-pressurized' by a single
261 packer to impose zero-flow increase in stress on the borehole wall. As described above, the
262 resulting increase in total stress adjacent to the packer causes a decrease in BEC. Compression of
263 the pore space adjacent to the packer will induce a pore pressure gradient, causing pore water to
264 migrate down gradient at a rate that is dependent on permeability. As pore water migrates down
265 gradient, pore pressure decreases, thereby increasing the effective stress on the rock matrix,
266 increasing compression of compliant pore spaces, and decreasing the BEC. If ERT
267 measurements were collected fast enough to sense the time-evolution of the BEC anomaly, those
268 measurements could conceptually be used to estimate in-situ intrinsic permeability of host rock
269 near the pressurized interval.

270 **8 Conclusions**

271 At the field scale, we have demonstrated the sensitivity of BEC to changes in stress in saturated
272 crystalline rocks that have been widely observed in laboratory scale settings. The relationship
273 between increases in stress and decreases in BEC enabled time-lapse ERT to image, in 3D, the
274 effective stress perturbation that developed around a set of pressurized borehole packers.
275 Imaging results provided information regarding the location and orientation of a relatively
276 compliant region of rock that ultimately fractured during hydrostimulation and provided the
277 primary flow pathway. These results speak to the possibility of enabling enhanced
278 understanding and control by using electrical and electromagnetic geophysical sensing methods
279 to remotely monitor stress and flow-path evolution in deep subsurface reservoirs (i.e. enhanced
280 geothermal, carbon sequestration, and oil and gas).

281 **Acknowledgments**

282
283 This material was based upon work supported by the U.S. Department of Energy, Office of
284 Energy Efficiency and Renewable Energy (EERE), Office of Technology Development,
285 Geothermal Technologies Office, under Award Number DE-AC05-76RL01830. The United
286 States Government retains, and the publisher, by accepting the article for publication,
287 acknowledges that the United States Government retains a non-exclusive, paid-up,
288 irrevocable, world-wide license to publish or reproduce the published form of this manuscript, or
289 allow others to do so, for United States Government purposes.

290 Sandia National Laboratories is a multimission laboratory managed and operated by
291 National Technology & Engineering Solutions of Sandia, LLC, a wholly owned subsidiary of
292 Honeywell International Inc., for the U.S. Department of Energy's National Nuclear
293 Security Administration under contract DE-NA0003525.

294 This paper describes objective technical results and analysis. Any subjective views or opinions
295 that might be expressed in the paper do not necessarily represent the views of the
296 U.S. Department of Energy or the United States Government. The research supporting
297 this work took place at the Sanford Underground Research Facility in Lead, South Dakota.
298 The assistance of the Sanford Underground Research Facility and its personnel in providing
299 physical access and general logistical and technical support is gratefully acknowledged.
300

301 **Open Research**

302 ERT monitoring data, meta data, and E4D ERT data processing files may be accessed through
303 the U.S. Department of Energy Geothermal Data Repository at
304 <https://gdr.openei.org/submissions/1480>. E4D source code and documentation is available at
305 <https://e4d.pnnl.gov>. Flow and pressure data collected during testing may be accessed through
306 the Geothermal Data Repository at <https://dx.doi.org/10.15121/1988394>.

307 **Figures**

308 **Figure 1.** A) Plan and B) Oblique views of the experimental testbed including borehole
309 orientations with ERT and seismic instrumentation locations. Intervals I1-I6 (black and green) in
310 A) denote isolated sections of borehole TC that were pressurized during shear stimulation
311 attempts. The inset image in B) is a photograph taken during testbed construction, standing in
312 the drift at -917 m northing and facing northward. Kickoff points for Site B boreholes are
313 located within the white outline.

314 **Figure 2.** Flowrate and interval pressure for shear stimulation attempt in wellbore Tc interval I1
315 (Figure 1A). Flowrate variations during the first ~20 minutes occur during interval pressure-up
316 (i.e. there is no flow into the formation).

317 **Figure 3.** ERT-derived changes in BEC during shear stimulation attempts in intervals 1-4.
318 Decreases in BEC are caused by stress-induced decreases in porosity around the pressurized
319 interval.

320 **Figure 4.** ERT-derived changes in BEC during shear stimulation attempts in intervals 5 and 6
321 (4A and 4B) and during the hydrofracture stimulation (4C). Decreases in BEC are caused by
322 stress-induced decreases in porosity around the pressurized interval. The annotated 'lobe' feature
323 observed during shear stimulation attempts 4-6 (Figures 3D, 4A and 4B) is co-located with the
324 projection of the hydrofracture from the injection interval to the break through point on wellbore
325 AMU.
326

327 **References**

- 328 Augustine, C. (2016). Update to Enhanced Geothermal System Resource Potential Estimate, *GRC Transactions*,
329 40(6).
- 330 Brace, W. F. (1975). Dilatancy-Related Electrical-Resistivity Changes in Rocks. *Pure and Applied Geophysics*,
331 113(1-2), 207-217. doi:DOI 10.1007/Bf01592911
- 332 Brace, W. F., & Orange, A. S. (1966). Electrical Resistivity Changes in Saturated Rock under Stress. *Science*,
333 153(3743), 1525-&. doi:DOI 10.1126/science.153.3743.1525
- 334 Brace, W. F., Orange, A. S., & Madden, T. R. (1965). Effect of Pressure on Electrical Resistivity of Water-Saturated
335 Crystalline Rocks. *Journal of Geophysical Research*, 70(22), 5669-+. doi:DOI 10.1029/JZ070i022p05669
- 336 Burghardt, J., Knox, H. A., Doe, T., Blankenship, D., Schwering, P., Ingraham, M., . . . Roggenthen, W. (2022).
337 *EGS Stimulation Design with Uncertainty Quantification at the EGS Collab Site*. Paper presented at the
338 American Rock Mechanics Association U.S. Rock Mechanics/Geomechanics Symposium, Santa Fe, New
339 Mexico.
- 340 Caddey, S. W., Bachman, R. L., Campbell, T. J., Reid, R.R., Otto, R. P. . (1991). *The Homestake gold mine, an
341 early Proterozoic iron-formation-hosted gold deposit, Lawrence County, South Dakota*. Retrieved from
342 <https://doi.org/10.3133/b1857J>
- 343 Davarpanah, S. M., Ván, P., & Vászárhelyi, B. (2020). Investigation of the relationship between dynamic and static
344 deformation moduli of rocks. *Geomechanics and Geophysics for Geo-Energy and Geo-Resources*, 6(1).
345 doi:ARTN 29
346 10.1007/s40948-020-00155-z
- 347 Fu, P. C., Schoenball, M., Ajo-Franklin, J. B., Chai, C. P., Maceira, M., Morris, J. P., . . . Team, E. C. (2021). Close
348 Observation of Hydraulic Fracturing at EGS Collab Experiment 1: Fracture Trajectory, Microseismic
349 Interpretations, and the Role of Natural Fractures. *Journal of Geophysical Research-Solid Earth*, 126(7).
350 doi:ARTN e2020JB020840
351 10.1029/2020JB020840
- 352 Heise, J. (2015). The Sanford Underground Research Facility at Homestake. *Proceedings of the South Dakota
353 Academy of Science, Vol 94, 94*, 347-347.
- 354 Johnson, T. C., Burghardt, J., Strickland, C., Knox, H., Vermeul, V., White, M., . . . Team, E. C. (2021). 4D Proxy
355 Imaging of Fracture Dilation and Stress Shadowing Using Electrical Resistivity Tomography During High
356 Pressure Injections Into a Dense Rock Formation. *Journal of Geophysical Research-Solid Earth*, 126(11).
357 doi:ARTN e2021JB022298
358 10.1029/2021JB022298
- 359 Johnson, T. C., & Wellman, D. (2015). Accurate modelling and inversion of electrical resistivity data in the
360 presence of metallic infrastructure with known location and dimension. *Geophysical Journal International*,
361 202(2), 1096-1108. doi:10.1093/gji/ggv206
- 362 Kaselow, A., & Shapiro, S. A. (2004). Stress sensitivity of elastic moduli and electrical resistivity in porous rocks.
363 *Journal of Geophysics and Engineering*, 1(1), 1-11. doi:Pii S1742-2132(04)73747-4
364 10.1088/1742-2132/1/1/001
- 365 Kneafsey, T. (2022). *The EGS Collab – Initial Results from Experiment 2: Shear Stimulation at 1.25 km depth*.
366 Paper presented at the 47th Workshop on Geothermal Reservoir Engineering, Sanford University.
- 367 Kneafsey, T. (2022). *The EGS Collab Project - Stimulations at Two Depths*. Paper presented at the ARMA
368 Geomechanics Symposium, Santa Fe, New Mexico.
- 369 Kneafsey, T., Blankenship, D., Burghardt, J., Johnson, T. C., Dobson, P. F., Schwering, P., . . . Robertson, M.
370 (2023). *The EGS Collab – Discoveries and Lessons from an Underground Experiment Series*. Paper
371 presented at the 48th Workshop on Geothermal Reservoir Engineering, Stanford, CA.
- 372 Min, K. B., Rutqvist, J., Tsang, C. F., & Jing, L. R. (2004). Stress-dependent permeability of fractured rock masses:
373 a numerical study. *International Journal of Rock Mechanics and Mining Sciences*, 41(7), 1191-1210.
374 doi:10.1016/j.ijrmms.2004.05.005
- 375 Pyrak-Nolte, L., DePaolo, D. J., Pietra, T. . (2015). *Controlling Subsurface Fractures and Fluid Flow: A Basic
376 Research Agenda*. . Retrieved from
- 377 Schmitt, D. R. (2015). Geophysical Properties of the Near Surface Earth: Seismic Properties. In G. Schubert (Ed.),
378 *Treatise on Geophysics* (2 ed., Vol. 11, pp. 43-87): Elsevier.
- 379 Zoback, M. D., & Byerlee, J. D. (1975a). Effect of Microcrack Dilatancy on Permeability of Westerly Granite.
380 *Journal of Geophysical Research*, 80(5), 752-755. doi:DOI 10.1029/JB080i005p00752

381 Zoback, M. D., & Byerlee, J. D. (1975b). Permeability and Effective Stress. *Aapg Bulletin-American Association of*
382 *Petroleum Geologists*, 59(1), 154-158.
383